ACS APPLIED MATERIALS & INTERFACES

Research Article

www.acsami.org

# Direct Coating Adherent Diamond Films on Fe-Based Alloy Substrate: The Roles of Al, Cr in Enhancing Interfacial Adhesion and Promoting Diamond Growth

X.J. Li,[†] L.L. He,*[,†] Y.S. Li,[‡,*,§] Q. Yang,[§] and A. Hirose[‡]

[†]Shenyang National Lab of Materials Science, Institute of Metal Research, University of Chinese Academy of Sciences, Shenyang 110016, China

[‡]Plasma Physics Laboratory, University of Saskatchewan, Saskatoon, Saskatchewan, Canada S7N 5E2

[§]Department of Mechanical Engineering, University of Saskatchewan, Saskatoon, Saskatchewan, Canada S7N 5A9

Supporting Information

**ABSTRACT:** Direct CVD deposition of dense, continuous, and adherent diamond films on conventional Fe-based alloys has long been considered impossible. The current study demonstrates that such a deposition can be realized on Al, Cr-modified Fe-based alloy substrate (FeAl or FeCrAl). To clarify the fundamental mechanism of Al, Cr in promoting diamond growth and enhancing interfacial adhesion, fine structure and chemical analysis around the diamond film−substrate interface have been comprehensively characterized by transmission electron microscopy. An intermediate graphite layer forms on those Al-free substrates such as pure Fe and FeCr, which significantly deteriorates the interfacial adhesion of diamond. In contrast, such a graphite layer is absent on the FeAl and FeCrAl substrates, whereas a very thin Al-rich amorphous oxide sublayer is always identified between the diamond film and substrate interface. These comparative results indicate that the Al-rich interfacial oxide layer acts as an effective barrier to prevent the formation of graphite phase and consequently enhance diamond growth and adhesion. The adhesion of diamond film formed on FeCrAl is especially superior to that formed on FeAl substrate. This can be further attributed to a synergetic effect including the reduced fraction of Al and the decreased substrate thermal-expansion coefficient on FeCrAl in comparison with FeAl, and a mechanical interlocking effect due to the formation of interfacial chromium carbides. Accordingly, a mechanism model is proposed to account for the different interfacial adhesion of diamond grown on the various Fe-based substrates.

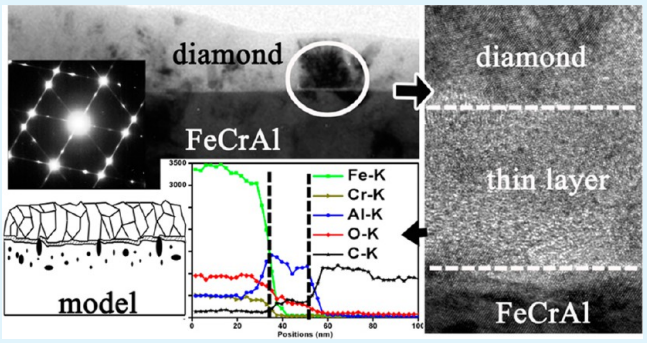


**KEYWORDS:** *diamond film, Fe-based substrate, Al, Cr alloying, interfacial adhesion, TEM*

## 1. INTRODUCTION

Fe-based alloys have gained a wide range of industrial applications because of their promising mechanical strength and relatively low cost, but accelerated damages occur and the service life is significantly shortened while they are used in harsh (wear, corrosive and erosive) environments. Especially, the early failure is usually initiated on the outermost surface of the substrate material, so it is extremely important to obtain strengthened surface for long-term high-performance service. Diamond films possess high hardness, chemical inertness and remarkable wear resistance, and they are considered one of the most attractive coating materials for surface protection.[1,2] Over the last 30 years, low-pressure and low-temperature chemical vapor deposition (CVD) of diamond films on a variety of substrate materials has been extensively developed.[3−10] However, it is still technologically difficult or even impossible to directly synthesize high-quality diamond films on the conventional Fe, Ni and Co-base alloy substrates.[11−16] The major barrier is closely associated with the intrinsic catalytic property of these transition metals, which induces preferential formation of voluminous graphite prior to diamond nucleation, and the weak bonded graphite at the diamond film/substrate interface usually leads to a spontaneous separation of the diamond film from the substrates. In addition, the difference of thermal expansion coefficients between diamond and the substrates is considerable (at room temperature, $\alpha_{diamond} \approx 0.8 \times 10^{-6}$ /K, $\alpha_{iron} \approx 11.8 \times 10^{-6}$ /K, data from Thermophysical Properties of Matter, The TPRC Data Series), which tends to induce large stresses that crack or delaminate the diamond film from the substrate.

Up to now, the main method to produce high quality diamond films on Fe, Co and Ni-base substrates is imposing an additional interlayer material such as Si, W, Mo, Ti, Cr, TiC, CrN, TiN, AlN, or multilayers Cu/Cr, Cr/Ti/TiC, and so

Received: May 7, 2013
Accepted: July 5, 2013
Published: July 5, 2013

  

on.[16−27] These interlayer materials are primarily applied to prevent carbon diffusion, suppress graphite formation, enhance diamond nucleation and reduce interfacial stress. Consequently, the interfacial adhesion of diamond films is enhanced. Nevertheless, this involves complex and costly multistep procedures, and the interfacial adhesions at both substrate/interlayer material and interlayer material/diamond film have to be simultaneously guaranteed. It should be simple and cost-effective to directly coat continuous and adherent diamond films on the alloy substrates, but little progress has been achieved so far.[13−15,28,29] Narayan et al.[28,29] first reported that the adhesion of diamond film directly grown on NiAl substrate could be significantly improved as a result of suppression of graphite formation at the diamond−substrate interface. They attributed that to the deactivated catalytic property of Ni, which was closely related to its altered 3d electronic structure after alloying with Al. However, this proposal is limited to a hypothesis and the actual mechanism has not been experimentally elucidated. Our recent investigations on diamond deposition on a series of transition metals and their alloys have also revealed that direct growth of adherent diamond films occurs only on those Al-containing substrates with a sufficiently high Al concentration.[30] Moreover, the critical fraction of Al required to obtain good interfacial adhesion of diamond films can be significantly reduced when Al and Cr are combined in the substrate.[30,31] As the interfacial adhesion property of diamond films is closely associated with the competitive growth of diamond and graphite which is further influenced by the substrate compositions, it is important to conduct detailed interfacial analysis so as to clearly clarify the related fundamental mechanism. Transmission electron microscopy (TEM) with a combination of real space imaging and spectroscopy is a perfect tool for such interfacial investigations. In the present paper, a detailed comparative study of diamond films formed on pure Fe, FeCr, FeAl, and FeCrAl alloy substrates is described, and the compositions and microstructures of the interfaces between the films and these alloy substrates have been extensively investigated by taking full advantage of TEM imaging capabilities. By correlating the TEM results with our previously obtained data on diamond nucleation, growth, and adhesion performances, we attempt to provide direct experimental evidence to interpret the enhanced interfacial adhesion mechanism of diamond films directly grown on Al-modified transition metal substrates.

## 2. EXPERIMENTAL SECTION

Diamond films were prepared by microwave plasma enhanced chemical vapor deposition (MPCVD). On pure Fe, Fe9Cr (wt %) and Fe25Al (wt %) alloy substrates, the films were deposited using a gas mixture of $H_2$ and 1 vol % $CH_4$. On Fe15Cr5Al (wt %) substrates, the films were deposited with a gas mixture of 1 vol % $CH_4/H_2$ and 20 vol % $CH_4/H_2$, respectively. These substrate materials were prepared by melting the desired amounts of the component metals using an arc-furnace under Ar protection. The substrates were machined into specimens with dimension of 10 mm × 10 mm × 1 mm and polished with 600 grit SiC paper, cleaned in acetone and finally dried in a $N_2$ flow. Diamond films deposition was performed in 2.45 GHz microwave plasma-assisted CVD apparatus (Plasmionique) using gas mixtures of $H_2$ and $CH_4$ with a total flow rate of 100 sccm. The base pressure was $1 \times 10^{-7}$ Torr and working pressure was maintained at 30 Torr. Microwave power was 800 W and substrate temperature was kept at 670 °C as measured by a thermocouple mounted underneath the stainless steel substrate holder. This temperature is about 80 °C lower than the diamond growth temperature on the substrate surface, which is directly exposed in plasma, as calibrated by optical spectroscopy.

Cross-sectional specimens for TEM observations were prepared by conventional method, i.e., by cutting, gluing, and grinding with silicon carbide paper, then dimpling to about 15 μm, and finally ion-milling by $Ar^+$ from both sides until some perforation occurred. A SUPRA35 field emission scanning electron microscope (SEM) was used to observe the surface morphology of the films. A Tecnai $G^2$ F20 transmission electron microscope was used at 200 kV for electron diffraction analysis and high-resolution transmission electron microscopy (HRTEM) observation. A Tecnai $G^2$ F30 transmission electron microscope, equipped with X-ray energy-dispersive spectrometer (EDS) systems and a postcolumn Gatan imaging filter (GIF 2000), was used at 300 kV for chemical composition analysis. The probe size for EDS line-scan was less than 2 nm and the step size about 2 nm. Energy-filtered images were performed using the three-window technique. To reduce the artifacts attributable to the effects of specimen drift, the frame acquisition time was less than 30 s.

## 3. RESULTS

**3.1. SEM Observation.** The SEM surface morphologies of the films formed on pure Fe, Fe9Cr, Fe25Al, Fe15Cr5Al alloy substrates are compared in Figure 1, with the insets showing

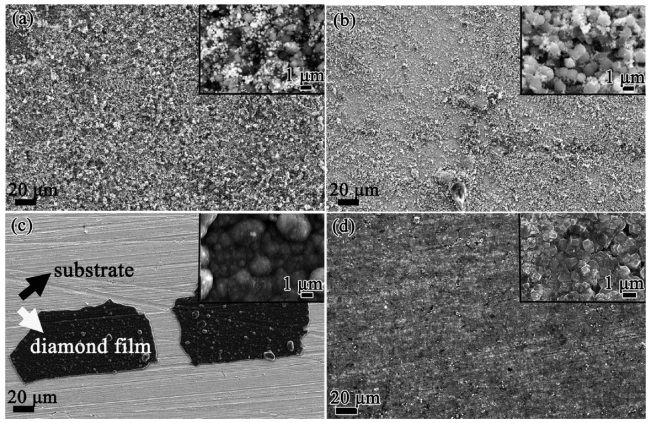


**Figure 1.** SEM images of the films formed on different substrates with a gas mixture of $H_2$ and 1 vol % $CH_4$, the insets show the magnified views of the films (plan-view): (a) on pure Fe substrate; (b) on Fe9Cr substrate; (c) on Fe25Al substrate; (d) on Fe15Cr5Al substrate.

the magnified views of the films. The film formed on pure Fe (Figure 1a) or FeCr alloy substrate (Figure 1b) has a poorly packed structure which can be easily removed in a supersonic water bath. On FeAl alloy substrate, the diamond film spalls locally after CVD, but the residual film is still stuck well to the substrate, as shown in Figure 1c, where the black arrow indicates the exposed substrate surface and the white arrow indicates the residual diamond film. On FeCrAl alloy substrate, the dense and continuous diamond film forms on the substrate (Figure 1d). In addition, Raman spectra of these films can be seen in Figure S1 (Supporting Information) and the detailed information can be referred to in our previous paper.[30−32]

**3.2. Identification of Al Effect by Comparing Pure Fe, FeCr, and FeCrAl Alloys.** The depositions of films on pure Fe, Fe9Cr and Fe15Cr5Al alloy substrates were carried out separately under the same conditions with a gas mixture of $H_2$ and 1 vol % $CH_4$. To confirm the alloying effect, we also changed the gas-phase chemistry on Fe15Cr5Al alloy substrate with a different gas mixture of 20 vol % $CH_4/H_2$. Detailed analysis results of microstructures and compositions are presented below.

*3.2.1. Structures of the Films Formed on Different Alloy Substrates.* Typical cross-sectional observations of the films formed on different alloy substrates are shown in Figure 2.

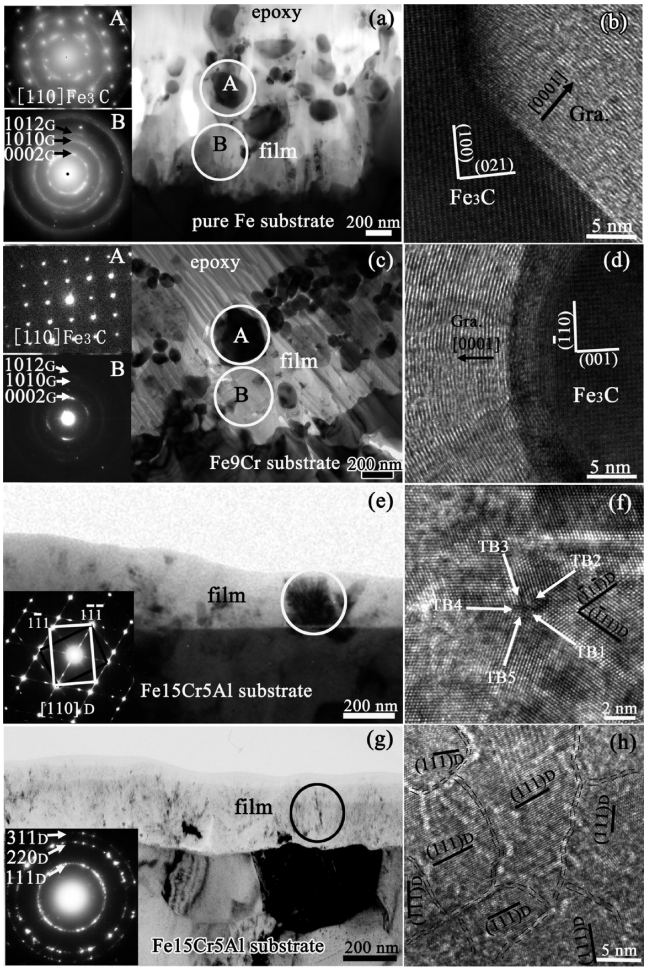


**Figure 2.** Typical cross-sectional observations of the films formed on different alloy substrates and different gas. (a–d) BF and HRTEM images about films formed on pure Fe substrate and Fe9Cr substrate respectively, with insets A and B showing the corresponding electron diffraction patterns (EDPs) of marked regions "A" and "B". These confirm that the films formed on non Al-containing substrates mainly consist of two phases: graphite and many carbide particles; (e–h) BF and HRTEM images about diamond films formed on Fe15Cr5Al substrate with 1 vol % $CH_4$ and 20 vol % $CH_4$, respectively, the insets are diamond diffraction patterns.

Figure 2a shows the cross-sectional bright-field (BF) image of the film formed on pure Fe substrate, with insets A and B corresponding to electron diffraction patterns (EDPs) of regions "A" and "B", respectively. They reveal that the film consists of two phases: graphite and many small iron carbide particles. In the film, the carbide particles are encapsulated by graphite layers and act as second nucleation sites for graphite (indicated by the HRTEM in Figure 2b). And similarly, the film formed on FeCr alloy substrate, illustrated in Figure 2c and d, has a similar structure as that formed on pure Fe substrate, including graphite and the carbides of the base metals. In contrast, dense and continuous diamond films formed on FeCrAl alloy substrate (Figure 2e–g). Figure 2e is the BF image of the film formed on FeCrAl alloy with 1 vol % $CH_4$, with the bottom inserted EDP indicating that the phase in the film is diamond. The columnar dark grain circled in the film is diamond in [110] axis, consisting of many stacking faults and twin defects. A typical HRTEM image of 5-fold twin is shown in Figure 2f, with the twin boundaries (TB) indicated by the white arrows. Besides, Figure 2g is the film formed on FeCrAl alloy with 20 vol % $CH_4$, as rings form in the diffraction pattern corresponding to diamond lattice spacing (see inset in Figure 2g). The film consists of very fine grains which are about 10–20 nm, as indexed in the HRTEM image in Figure 2h, which are much smaller than those in Figure 2e (about 200–300 nm), and furthermore, the comparison of grain sizes with different gas phase can be seen more clearly in the plan-view BF images of the films in Figure S2 (Supporting Information). These data indicate that adherent nanocrystalline diamond film has formed with a high $CH_4$ concentration.

*3.2.2. Carbide Precipitation Conditions in Different Alloy Substrates.* The conditions of carbides precipitated in pure Fe, FeCr and FeCrAl alloy substrates are very different. A continuous iron carbides layer formed in pure Fe substrate, as shown in Figure 3a. The inset shows the corresponding EDP

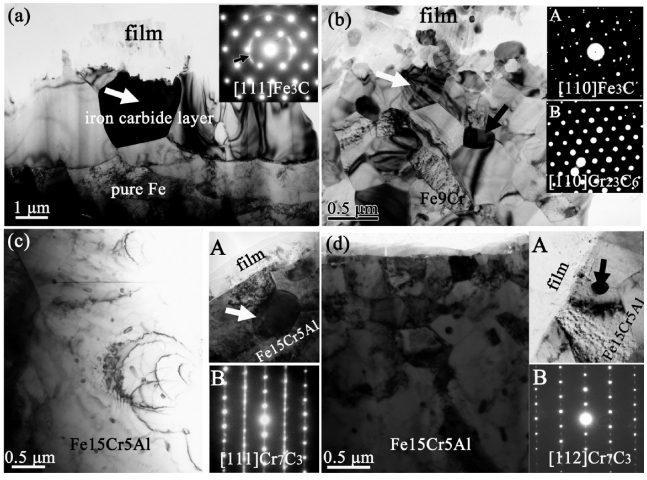


**Figure 3.** Comparison of the conditions of carbides precipitated in pure Fe, FeCr, and FeCrAl alloy substrates. TEM images and corresponding EDPs of (a) carbides precipitated in pure Fe substrate; (b) carbides precipitated in FeCr substrate; (c, d) carbides precipitated in FeCrAl substrate with 1 vol % $CH_4$ and 20 vol % $CH_4$, respectively.

of the white arrow marked carbide, which is identified as $Fe_3C$ phase, whereas the diffraction rings (indicated by the black arrow) in EDP are from the graphite phase in the film. In FeCr substrate, as shown in Figure 3b, a large number of iron carbides (marked by the white arrow and inset A is corresponding EDP) and chromium carbides (marked by the black arrow and inset B is corresponding EDP) formed, but no continuous carbides layer formed and the size of carbides is much smaller than that of carbides in pure Fe substrate. However, in FeCrAl substrate, only chromium carbides were observed at both low and high $CH_4$ concentrations, as shown in Figure 3c, d. A general low-magnification image illustrating the carbides precipitated condition in FeCrAl substrate with 1 vol % $CH_4$ is shown in Figure 3c, and a typical carbide particle is arrowed in the enlarged image of inset A, with its corresponding EDP (see inset B in Figure 3c) demonstrating that the carbide is $Cr_7C_3$ phase. Figure 3d shows that even with a much higher C concentration (20 vol % $CH_4$), only chromium carbides (as demonstrated by inset B in Figure


dx.doi.org/10.1021/am401709j | ACS Appl. Mater. Interfaces 2013, 5, 7370–7378

3d) were observed in FeCrAl substrate. In some cases, the carbides were preferentially precipitated along the crystal defects such as dislocations or crystal boundaries, as the marked carbide particle in inset A of Figure 3d.

*3.2.3. Detailed Microstructures of Interfaces.* The surfacial conditions of substrate critically influence the diamond nucleation during the process of diamond film deposition because the substrate surface absorbs and chemically interacts with the gas phase that diffuses to the surface.[33] Therefore, it is of extreme importance to thoroughly investigate the interfaces between different alloy substrates and films to clarify the alloying modification effect.

On pure Fe substrate, carbon atoms react with the surfacial Fe atoms and accordingly forms a continuous $Fe_3C$ layer of 2−3 $\mu$m in thickness (clearly shown in Figure 3a), and then the graphite film nucleates and grows on these iron carbides.[34] Figure 4 shows the typical structural information at the

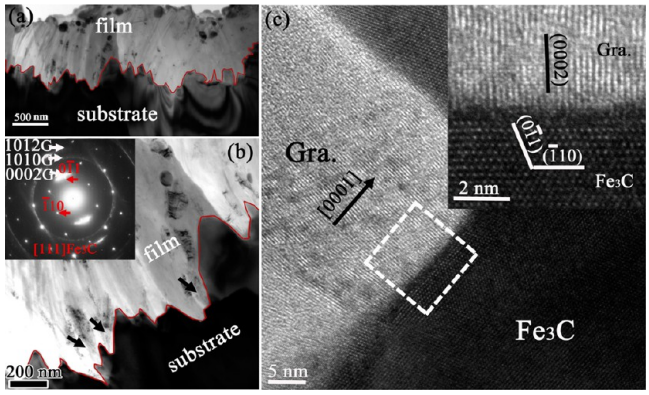


**Figure 4.** Detailed microstructures among the interface between pure Fe substrate and the film. (a) Low-magnification and (b) enlarged cross-sectional BF images, with inset showing the interfacial EDP, the interface as marked by the red curve is very rough, has an indented shape. (c) HRTEM image of the hollow area, showing the graphite phase directly grows from the substrate iron carbide.

interface between pure Fe substrate and the film. A low-magnification cross-sectional BF image is shown in Figure 4a, illustrating that the interface between the film and the substrate is very rough and has a serrated shape (marked by the red curve in Figure 4a, b). Figure 4b is an enlarged BF image of the typical region, clearly showing a preferential nucleation of graphite phases at the hollow sites of the serrated substrate surface (indicated by the black arrows in Figure 4b). The inset in Figure 4b is EDP taken from the interfacial region as marked by the black arrows. The main diffraction spots are formed by the substrate $Fe_3C$ along [111] axis, whereas the diffraction rings indicated by the white arrows in EDP represent the interfacial graphite phase. Figure 4c is the cross-sectional HRTEM image of the marked hollow area, showing that the graphite phase directly grows from the iron carbide, whereas no intermediate layer is observed in between. The top inset is an enlarged HRTEM image corresponding to the white dashed square, showing that the graphite phase with its (0002) plane approximately perpendicular to the $Fe_3C$ (110) surface, but the clear epitaxial orientation relationship between graphite and $Fe_3C$ is not observed.

Similarly, on FeCr alloy, the interfacial graphite phase also nucleates and grows on the substrate iron carbides and the detailed interfacial microstructure is similar to that on pure Fe.

Comparison with pure Fe and FeCr alloy, the interfacial microstructure on FeCrAl alloy is quite different, and these differences can provide direct evidence to understand the enhanced interfacial adhesion mechanism. Figure 5 shows the

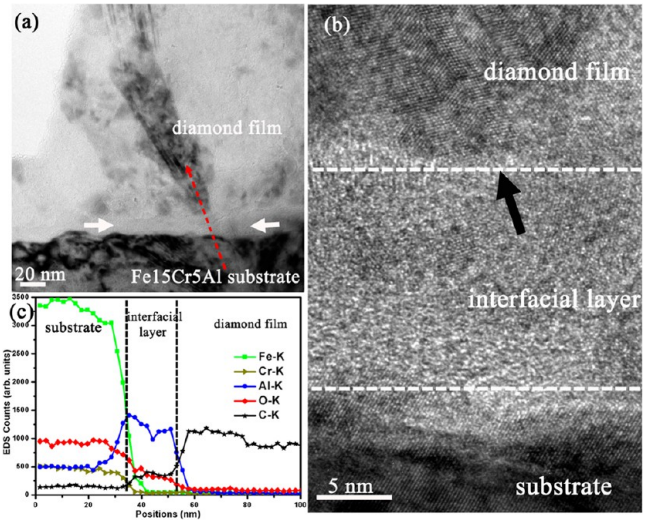


**Figure 5.** (a) Cross-sectional BF image of the diamond film prepared with 1 vol % $CH_4$ on Fe15Cr5Al substrate. (b) The interfacial HRTEM image, the arrow indicates the location where the diamond crystalline starts growing on top of the amorphous phase. (c) EDS line-scan profile scanned along the red dashed arrow indicated in a. There exists an interfacial layer where Al element content is much higher.

typical microstructure and composition information at the interface between FeCrAl substrate and diamond film prepared with 1 vol % $CH_4$. Figure 5a is a low-magnification cross-sectional BF image. The dark part at the bottom of the image is FeCrAl substrate; the upper part is the film consisting of several diamond crystals, and the column diamond crystal in the film is along [110] axis. Between the substrate and the film, there is a narrow interfacial layer indexed by white arrows in the image. A HRTEM image of the interfacial layer suggests the interfacial layer is amorphous with some small ordered islands, and the thickness is about 10−15 nm, as shown in Figure 5b. The upper part is the diamond crystal, and the black arrow indicates the location where the diamond crystalline column starts growing on the top of this amorphous layer. Figure 5c is an EDS line-scan profile, scanned along the red dashed arrow indicated in Figure 5a. The plots at the left side result from the scanning of FeCrAl substrate and at the right side show the results of diamond film. The interfacial layer is separated by the vertical lines in the EDS line-scan profile. In this region, the content of element Al is much higher than that in the substrate, whereas there is nearly no Fe and Cr. These data imply that a thin Al-rich amorphous interfacial layer with several nanometers in thickness formed along the FeCrAl substrate/diamond film interface. In the substrate, the concentration of oxygen appears relatively high, however, this is an artifact by Cr. Cr-L2,3 peak is 584 eV, whereas O−K peak is 532 eV, which can not be distinguished by EDS (resolution is about 100 eV), so their peak is overlapped.

Figure 6 shows the interfacial conditions of the diamond film prepared on FeCrAl substrate with 20 vol % $CH_4$. Figure 6a is a low-magnification cross-sectional BF image showing both the top ultrafine diamond crystallites and the underlying FeCrAl


dx.doi.org/10.1021/am401709j | ACS Appl. Mater. Interfaces 2013, 5, 7370−7378

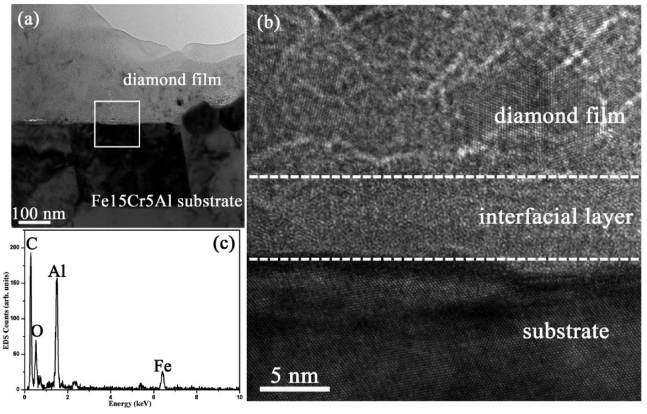


**Figure 6.** (a) Cross-sectional BF image of the interfacial area in the sample prepared with 20 vol % $CH_4$ on Fe15Cr5Al substrate. (b) HRTEM image of the interface, the substrate is $\alpha$-Fe along the [100] axis, an amorphous layer exist between the diamond film and the substrate; (c) an EDS point-scan profile scanned across the interface, showing the Al element concentration in the amorphous layer.

substrate. A HRTEM image (Figure 6b) shows the details of the interfacial area indicated by the square in Figure 6a. The nanocrystal diamond phase in the film is identified by an interplanar spacing which is about 0.205 nm, and the substrate is $\alpha$-Fe in [100] axis. Between the film and the substrate exists an amorphous interfacial layer, with thickness of 3−5 nm, which is much thinner than that formed with 1 vol % $CH_4$. The composition of this interfacial layer shown in Figure 6c indicates that it is also an Al-rich oxide layer. The counts of C and Fe were assumed to originate from the film and the substrate, respectively.

Energy-filtered transmission electron microscopy (EFTEM) is a parallel imaging technique,[35] which only gathers images from scattered electrons of a specific energy-loss range. It can easily and quickly achieve a high spatial resolution in nanoscale. Therefore, this technique is very appropriate for investigating the elemental distribution in the narrow interfacial layer between FeCrAl substrate and diamond film. The area enclosed by the square in Figure 6a has been examined, and the results are shown in Figure 7. Figure 7a is the BF image filtered with zero loss peak (ZLP), where the interfacial layer shows a bright contrast. The corresponding energy-filtered mappings are shown in Figure 7b−e. The elemental spatial distribution is clearly visible by combining these mappings. The red dash lines indicate the boundaries of Fe (Figure 7b, substrate) and C (Figure 7c, film) maps, and obviously, a narrow interfacial layer exists between the two red dash lines. Figure 7d is the Al distribution map, and the red arrow denotes the layer where Al is enriched. The position of this denoted layer is consistent with the narrow interfacial layer. Furthermore, a color mixed RGB image is shown in Figure 7f with Fe (green), Al (blue) and C (red). It clearly demonstrates that the interfacial area is an Al-rich layer. In addition, the O element distribution (Figure 7e) is nearly the same as that of Al, revealing that probably the Al element in this interfacial area exists in an oxide form. It is worth noting that the Cr element map is not included here because most of Cr element has formed into carbides.

Many chromium carbides precipitated at the interface between FeCrAl substrate and diamond film, and it is interesting to point out that there is also an Al-rich layer on these interfacial chromium carbides. Figure 8a is the BF image of interfacial chromium carbide filtered with ZLP, and the corresponding energy-filtered mappings are shown in Figure 8b−f, with the white arrows indicating the carbide position. The elemental mappings indicate that a thin layer still exists on the top of the chromium carbide where both Al and O are enriched.

**3.3. Identification of Cr Effect by Comparing FeAl and FeCrAl Alloys.** Although the interfacial adhesion of diamond films formed on those Al-containing substrates are considerably improved in comparison with those on Al-free substrates, the diamond film formed on FeAl substrate still suffers from local spallation after CVD, as shown in Figure 1c. The cross-sectional BF interfacial images of the residual diamond film (the black arrow indicated in Figure 1c) grown on FeAl substrate is shown in Figure 9. In some cases, the residual film is adherent with the FeAl substrate, as shown in Figure 9a. The top inset is the EDP of the residual film, which further confirms that the film formed on FeAl substrate is the diamond phase, consistent with our

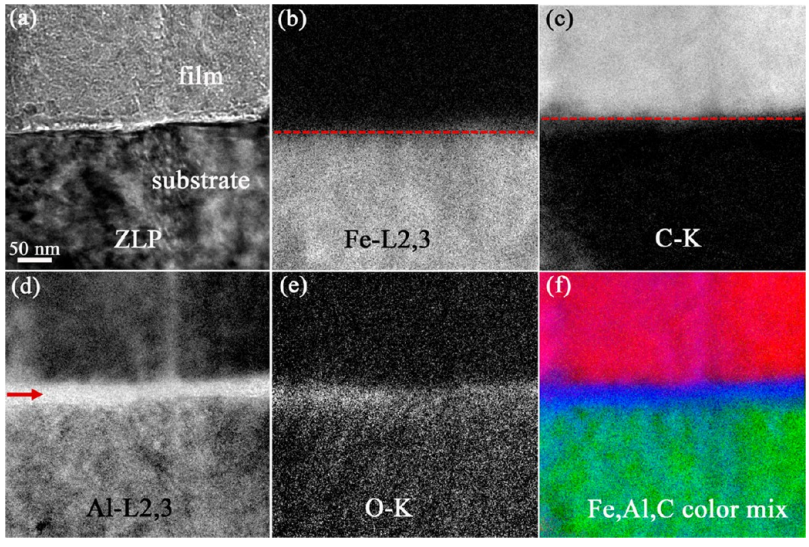


**Figure 7.** EFTEM images of the FeCrAl/diamond interface demonstrating Al enrich in the interfacial layer. (a) BF image filtered with ZLP; (b) Fe-L2,3 map; (c) C−K map; (d) Al-L2,3 map; (e) O−K map; (f) color mixed RGB image with Fe (green), Al (blue), C (red).


dx.doi.org/10.1021/am401709j | ACS Appl. Mater. Interfaces 2013, 5, 7370−7378

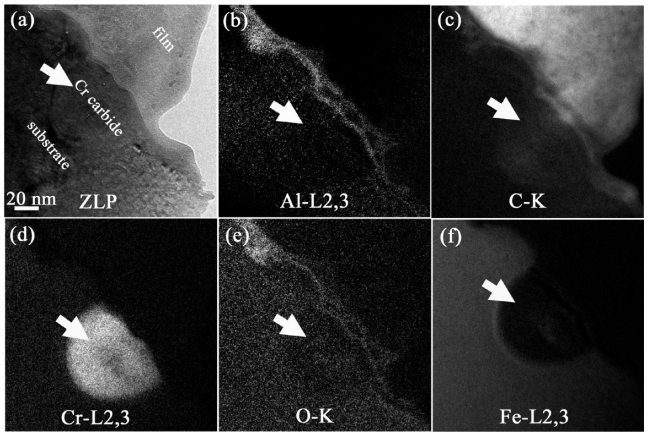


**Figure 8.** (a) BF image of chromium carbide precipitated along the FeCrAl/diamond interface filtered with ZLP; (b) Al-L2,3 map; (c) C–K map; (d) Cr-L2,3 map; (e) O–K map; (f) Fe-L2,3 map; the white arrows indicate the carbide position.

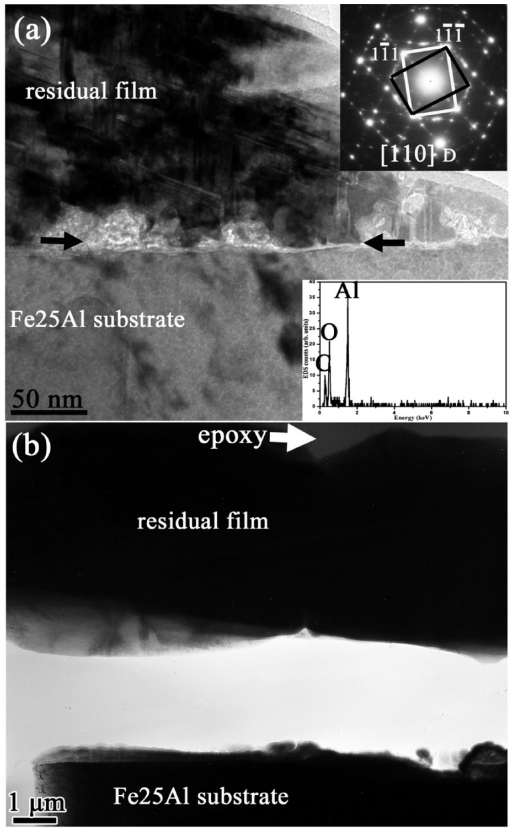


**Figure 9.** Cross-sectional TEM observations of the residual diamond film (marked by the white arrow in Figure 1c on Fe25Al substrate. (a) The residual diamond film adheres to the substrate, with the top inset showing the EDP of the residual film and the bottom inset showing the composition of the marked interface. (b) The residual diamond film is detached from the substrate by the glue.

previous Raman analysis.[30] The bottom inset shows the composition of the arrowed interface, indicating that there is an Al-rich layer between FeAl substrate and diamond film. However, in many cases, the residual film is removed away from the substrate by the glue (epoxy) during the preparation of cross-sectional TEM samples, as shown in Figure 9b. This indicates that the adhesion strength between the residual film and FeAl substrate is not strong. In contrast, diamond film could grow densely, continuously and adherently on FeCrAl substrate (Figure 1d). And on the basis of our large numbers of TEM observations, no films have been adhesive away from the substrate by the glue, suggesting the interfacial adhesion between diamond film and FeCrAl substrate is much strong in comparison with FeAl substrate. Furthermore, indentation and scratch tests (see Figure S3 in the Supporting Information) also demonstrate the excellent interfacial adhesion between diamond film and FeCrAl substrate, and the detailed mechanical testing information can be referred to in our previous paper.[32]

*3.3.1. Estimation of Thermal Stresses.* During heating or cooling, high stresses are induced in the coating if the thermal-expansion coefficients of the diamond films and the Fe-based alloy substrates vary significantly from each other. The thermal stress can be readily estimated from the equation[36]

$$\sigma_{\text{thermal}} = \frac{E}{1-\upsilon}\int_{20}^{T}(\alpha_{\text{f}} - \alpha_{\text{s}})dT$$

Where $E$ is Young's modulus of diamond, about 1050 GPa; $\alpha_{\text{f}}$ and $\alpha_{\text{s}}$ are the thermal-expansion coefficients of the diamond film and substrate, respectively; $\upsilon$ (= 0.07) is the Poisson ratio of the diamond film, and $T$ (about 670 °C) is the deposition temperature. The estimated thermal stresses between the diamond films and the different substrates by the equation are given in Table 1.

**Table 1. Thermal Stress of Diamond Films on Various Substrates Were Estimated**

| | $\alpha \times 10^{-6a}$/K | | | |
|---|---|---|---|---|
| material | 293 K | 943 K | $\alpha_{\text{ave}}$ | $\sigma_{\text{thermal}}$ (GPa) |
| diamond | ~0.8 | ~4.2 | ~2.5 | |
| Fe | ~11.8 | ~16.5 | ~14.2 | ~8.59 |
| Cr | ~4.9 | ~11.5 | ~8.2 | ~4.18 |
| Al | ~23.1 | ~32.3 (800 K) | ~28 | ~18.7 |
| Fe15Al | ~11.6 | ~21 | ~16.3 | ~10.13 |
| Fe25Al | | | | ≫10.13 |
| Fe15Cr | ~10.5 | ~13.7 | ~12.1 | ~7.04 |
| Fe15Cr5Al | | | | 8.59 > $\sigma$ > 7.04 |

[a] $\alpha$ is the linear thermal expansion coefficient (data from Thermophysical Properties of Matter, The TPRC Data Series).

The thermal-expansion coefficient of Fe25Al is not available, but it must be greater than that of Fe15Al, as the thermal-expansion coefficient of Al is much higher than that of Fe. Hence, the thermal stress is larger than 10.13 GPa. Similarly, the thermal-expansion coefficient of Fe15Cr5Al is also inaccessible. By comparing with Fe15Cr and taking into account only a small amount of Al added, the thermal stress is estimated to be about 7.5–8.5 GPa, which is larger than that on Fe15Cr substrate and lower than that on pure Fe substrate.

*3.3.2. Interfacial Cr Carbides.* Many chromium carbide particles have formed at the interface between FeCrAl substrate and diamond film. Figure 10a, b shows the BF images of chromium carbides precipitated at the FeCrAl/diamond interface, with the insets showing the corresponding EDPs of the marked carbides. Interestingly, in some cases, the interfacial carbides are partially immerged in the substrate, whereas the rest are incorporated into the diamond film (arrows indicated carbides in Figure 10a, b), which act as pegs at the interface and


dx.doi.org/10.1021/am401709j | ACS Appl. Mater. Interfaces 2013, 5, 7370–7378

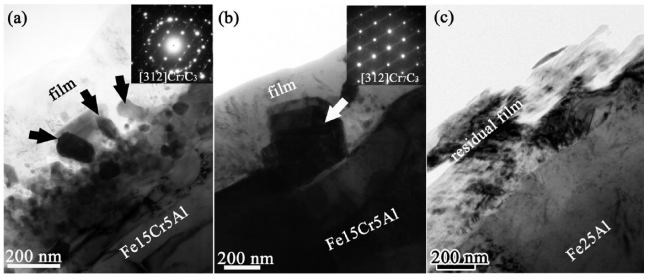


**Figure 10.** (a, b) BF images and corresponding EDPs of chromium carbides precipitated along the FeCrAl/diamond interface; (c) BF image of the FeAl/diamond interface, no carbide was observed.

significantly enhance the interfacial bonding strength between the diamond film and the substrate. In contrast, no carbide phase has been observed along the FeAl/diamond interface, as indicated by Figure 10c.

## 4. DISCUSSION

**4.1. Role of Al.** Comparison of the films formed directly on pure Fe, FeCr, FeAl and FeCrAl substrates, Fe-based alloy substrate alloyed with Al has been proved favorable for promoting diamond growth and enhancing interfacial adhesion. On Al-free substrates such as pure Fe and FeCr, the formed films (Figure 1a, b) have a poorly packed structure and mainly consist of graphite and many small carbide particles (Figure 2a–d). Only after prolonged deposition time, diamond films can form on these substrates but spontaneously delaminate from the substrates after cooling.[31] Two major barriers that have restricted adherent diamond coating directly on Fe substrate are the high diffusion coefficient of carbon in iron and the strong catalytic effect of iron for preferential graphite formation. On the one hand, there is not an effective interfacial layer available on pure Fe substrate to hinder C diffusion, hence C will quickly diffuse into the Fe substrate and lead to substrate carbonization (Figure 3a). On the other hand, Fe also diffuses outward and the interfacial products formed on the substrate surface usually consist of both graphite and iron carbides (Figure 2a). And these iron carbide particles in the film further act as second nucleation sites for graphite (Figure 2b). The addition of Cr alone to Fe substrate does not significantly improve diamond growth and adhesion, and the interfacial products formed on FeCr alloy are very similar to those on pure Fe substrate, as shown in Figure 2c, d. The only difference is that the continuous $Fe_3C$ layer formation on FeCr alloy is hindered (Figure 3b) because of a stronger carbide forming ability of Cr in comparison with Fe. After alloying modification by Al element, a very thin Al-rich interfacial oxide layer forms on the substrate surface during the process of film deposition. The comprehensive HRTEM (Figures 5b and 6b) observation of the interface between FeCrAl substrate and diamond film reveals that an amorphous interfacial layer has formed. The EDS (Figures 5c and 6c) and EFTEM (Figure 7) analysis further demonstrate that this interfacial layer is especially rich in Al, along with a simultaneous O enrichment. Accordingly, the element Al is assumed to be an amorphous alumina in the interfacial layer. From our EDS profiles of interfacial layer, the Al/O ratio of the amorphous interfacial layer can be quantified to be about 2:3, and oxidation-induced amorphization of Al has been observed by both experiments and molecular-dynamics simulations.[37−39] The Al oxide interfacial layer in situ formed on FeCrAl substrate surface plays critical roles in enhancing diamond nucleation, growth and adhesion. Comparing the carbides precipitated conditions in FeCr and FeCrAl substrate (Figure 3b–d), large numbers of chromium carbides and iron carbides formed in FeCr substrate, while only chromium carbides formed in FeCrAl substrate, implying that the Al oxide layer on FeCrAl substrate effectively impedes the surfacial carbon diffusing into the substrate. Meanwhile, the Al oxide layer acts as a highly protective layer to effectively separate the carbonizing atmosphere from the alloy substrate and decrease the surfacial activity of Fe. Therefore, the graphite catalyzing effect by iron is effectively hindered. Furthermore, a high surfacial concentration of C normally promotes diamond nucleation and growth.[40] Once an Al oxide layer forms on the substrate surface, the diffusion of C atoms toward the substrate is greatly decreased. Consequently, carbon atoms primarily accumulate on the substrate surface and quickly approach a supersaturated level, which is very favorable for the nucleation and subsequent growth of exclusive diamond film.

The formation of the intermediate Al oxide layer may come from two sources. On the one hand, because of the high reactivity of Al to oxygen, the Al oxide passivation thin layer can even form at ambient atmosphere. On the other hand, before diamond nucleation starts in the CVD deposition process, an incubation period exists which may range from a few minutes to hours, depending on substrate materials, surface pretreatment and deposition parameters.[33] The incubation period provides time for the oxidation of aluminum, where oxygen comes from the impurity of the reaction gases. With 20 vol % $CH_4$, C will accumulate more quickly on the substrate surface, and thus less time is required to meet the supersaturation condition for diamond nucleation. Accordingly, the incubation period is shorter than that with 1 vol % $CH_4$. Once diamond starts to grow, the oxidation speed of aluminum on the substrate surface will be decelerated and finally terminated. As a result, with 20 vol % $CH_4$, the interfacial Al oxide layer would be thinner than that with 1 vol % $CH_4$. This assumption is in accordance with our experimental results. For instance, the thickness of the interfacial oxide layer is about 3–5 nm (Figure 6b) with 20 vol % $CH_4$, whereas it is about 10–15 nm with 1 vol % $CH_4$ (Figure 5b).

**4.2. Role of Cr.** Although FeCr alloy does not provide significant improvement in the interfacial adhesion of diamond films, the presence of chromium in FeCrAl ternary alloy demonstrates a beneficial effect in a few aspects. In our previous work,[30] only a higher Al content in FeAl alloys could effectively eliminate the formation of nondiamond phase on the substrate surface. After Cr addition, a much smaller amount of Al is needed to form continuous and adherent diamond films. This phenomenon can be explained by the third element effect (TEE). The third element (chromium) can boost the formation of the Al-oxidized scale on the surface up to such a level that the Al content in bulk can be kept within the acceptable limits regarding the mechanical properties of the alloy.[41−45]

Besides, element Cr plays an important role in enhancing the interfacial adhesion between the diamond film and the substrate. The thermal-expansion coefficient of Fe25Al alloy is much larger than that of Fe (see Table 1). Because of the large difference in the thermal expansion of diamond and Fe25Al substrate, the stresses generated in the diamond film after cooling to room temperature are very large (>10 GPa). The large stresses frequently induce cracking or delamination of diamond films from the substrate. Therefore, the diamond film formed on Fe25Al substrate easily suffers from a local spallation

(as shown in Figure 1c), and the residual film is also easily detached from the substrate (Figure 9b). However, the thermal stresses between diamond film and Fe15Cr5Al (about 7.5−8.5 GPa) are much smaller than that of Fe25Al, which can be attributed to the fact that the thermal-expansion coefficient of Cr is much lower than that of Al, and also lower than that of Fe (see Table 1). Meanwhile, as Cr added, the Al content needed for ensuring the diamond formation is remarkably reduced. Moreover, the interfacial carbides may play very positive roles in the mechanical interlocking of the film and the substrate. A comparative study on the interfaces (Figure 10) has revealed that many Cr carbides precipitated at the FeCrAl−-diamond interface, whereas there is not any carbide formed at the FeAl−-diamond interface. The Cr carbides formed along the film/substrate interface act as pegs to hinder the film detaching from the substrate. Because of the strong mechanical interlocking and chemical bonding by these interfacial carbides, the adhesion between diamond film and FeCrAl substrate is greatly enhanced. This is consistent with other researchers applying Cr as interlayer to improve the interfacial adhesion.[20,23,46] Finally, a large number of carbide particles also precipitate along the crystal defects such as dislocations and crystal boundaries in the near surface of the substrate (Figure 3d), otherwise these defects are short channels for rapid carbon diffusion. By hindering carbon diffusing deep into the substrate, these carbide particles also play an auxiliary role in the accumulation of C concentration in the surface.

**4.3. A Simple Model.** On the basis of our analysis and discussion, a model describing the mechanism of diamond films grown on Al, Cr modified Fe-based substrate is proposed, as shown in Figure 11:

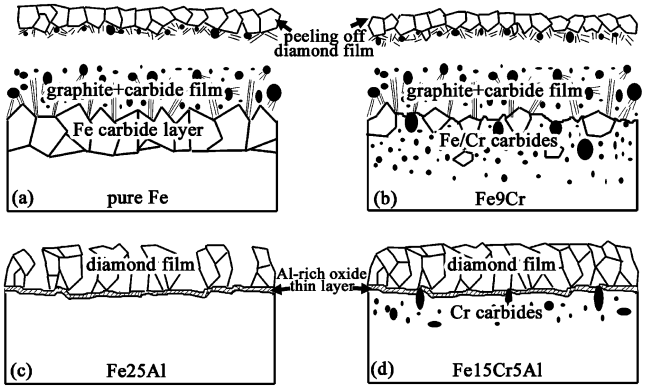


**Figure 11.** Model describing the mechanism of diamond films grown on Al, Cr-modified Fe-based substrate is proposed.

(a) On pure Fe substrate, after prolong time deposition, the continuous diamond film can form, but it spontaneously peels off the substrate after cooling, whereas the interfacial products that remain on the substrate surface consist of loosely packed graphite and iron carbide particles. A continuous iron carbide layer forms in the substrate as well.

(b) On Fe−Cr alloy substrate, the film structure is quite similar to that observed on pure Fe, with peeled outermost diamond film, an intermediate graphite layer on the substrate surface, and the carbides of the base metals.

(c) On Fe−Al binary alloy substrate, the graphite intermediate layer is absent, whereas an Al-rich interfacial oxide layer is observed. The interfacial adhesion of diamond film is improved but the film still spalls locally.

(d) On FeCrAl ternary alloy substrate, the graphite intermediate phase is prevented and a better adherent diamond film forms. An Al-rich oxide layer forms along the interface, with chromium carbides precipitated at the interface and the near surface of the substrate.

In this model, it is necessary to emphasize that although a diamond layer can also form on pure Fe or FeCr substrate after long time deposition, it easily peels off upon cooling because of the graphite intermediate layer. The key role of Al is that an Al-rich oxide layer forms at the interface, which acts as (i) an efficient barrier for both C and Fe diffusion; (ii) a crucial hindrance of Fe catalyzed preferential formation of graphite; (iii) a quick accumulation of C for supersaturation. Meanwhile, the supplementary role of Cr is to (i) reduce the critical Al concentration required to form its oxide; (ii) enhance the interfacial adhesion through decreasing the thermal stresses and providing mechanical interlocking by the interfacial chromium carbides; (iii) play an auxiliary role in the accumulation of surfacial C concentration. Therefore, the beneficial roles of element Al and Cr, especially their synergetic effects, enable a dense, continuous, and adherent diamond film to form on FeCrAl alloy substrate.

## 5. CONCLUSIONS

Direct CVD growth of adherent diamond films on conventional Fe-based alloys is difficult, but it is possible by alloying the substrates with element Al, especially a combination of Al and Cr. Comprehensive TEM interfacial analysis reveals that on pure Fe and FeCr alloy substrates, an intermediate graphite layer forms between the diamond film−substrate interface, with a simultaneous carbonization attack in the substrates. Therefore, diamond films formed are not adherent to these substrates because of the weak interfacial bonding caused by the intermediate graphite phase. In contrast, the formation of graphite phase is absent on the Al-containing Fe-based alloy substrates. Instead, a very thin amorphous Al-rich oxide layer is in situ formed between the diamond film and substrate interfaces. This Al-rich interfacial oxide layer acts as an effective barrier to hinder the diffusion of carbon and suppress the formation of graphite. Accordingly, an enhanced interfacial adhesion is obtained on the Al-modified substrates. Furthermore, the interfacial adhesion of diamond films directly grown on FeCrAl substrate shows superior to that grown on FeAl. This can be attributed to the decreased substrate thermal-expansion coefficient after Cr addition and the enhanced mechanical interlocking adhesion provided by the interfacial chromium carbides.

## ■ ASSOCIATED CONTENT

### Supporting Information

Raman spectra of films formed on different substrates; plan-view bright-field TEM images of the films formed on different substrates; and mechanical characterization of diamond film formed on Fe15Cr5Al substrate. This material is available free of charge via Internet at http://pubs.acs.org.

## AUTHOR INFORMATION


### Corresponding Author

*E-mail: llhe@imr.ac.cn (L.L.H.). Phone: +86-24-2397-1841.


### Notes

The authors declare no competing financial interest.

## ACKNOWLEDGMENTS

This work was supported by the national basic research program of China (Grant 2011CB605803 and 2011CB605604), and the Canada Research Chair Program and the Natural Sciences and Engineering Research Council of Canada (NSERC).

## REFERENCES


(1) Singh, R. K.; Gilbert, D. R.; Fitz-Gerald, J.; Harkness, S.; Lee, D. G. *Science* **1996**, *272*, 396.

(2) Lee, S. T.; Lin, Z.; Jiang, X. *Mater. Sci. Eng., R* **1999**, *25*, 123.

(3) Tachibana, T.; Yokota, Y.; Miyata, K.; Onishi, T.; Kobashi, K.; Tarutani, M.; Takai, Y.; Shimizu, R.; Shintani, Y. *Phys. Rev. B* **1997**, *56*, 15967.

(4) Liu, W.; Yang, P. C.; Wolden, C. A.; Davis, R. F.; Prater, J. T.; Sitar, Z. *J. Appl. Phys.* **1998**, *83*, 7658.

(5) Yoshimoto, M.; Yoshida, K.; Maruta, H.; Hishitani, Y.; Koinuma, H.; Nishio, S.; Kakihana, M.; Tachibana, T. *Nature* **1999**, *399*, 340.

(6) Lee, S. T.; Peng, H. Y.; Zhou, X. T.; Wang, N.; Lee, C. S.; Bello, I.; Lifshitz, Y. *Science* **2000**, *287*, 104.

(7) Sawada, H.; Ichinose, H.; Watanabe, H.; Takeuchi, D.; Okushi, H. *Diamond Relat. Mater.* **2001**, *10*, 2030.

(8) Kiselev, N. A.; Hutchison, J. L.; Roddatis, V. V.; Stepanova, A. N.; Aksenova, L. L.; Rakova, E. V.; Mashkova, E. S.; Molchanov, V. A.; Givargizov, E. I. *Micron* **2005**, *36*, 81.

(9) Schreck, M.; Hormann, F.; Gsell, S.; Bauer, T.; Stritzker, B. *Diamond Relat. Mater.* **2006**, *15*, 460.

(10) Almeida, F. A.; Oliveira, F. J.; Silva, R. F.; Baptista, D. L.; Peripolli, S. B.; Achete, C. A. *Appl. Phys. Lett.* **2011**, *98*, 171913.

(11) Ong, T. P.; Chang, R. P. H. *Appl. Phys. Lett.* **1991**, *58*, 358.

(12) Kawarada, M.; Kurihara, K.; Sasaki, K. *Diamond Relat. Mater.* **1993**, *2*, 1083.

(13) Zhu, W.; Yang, P. C.; Glass, J. T.; Arezzo, F. *J. Mater. Res.* **1995**, *10*, 1455.

(14) Mallika, K.; Ramamohan, T. R.; Jagannadham, K.; Komanduri, R. *Philos. Mag. B-Phys. Condens. Matter Stat. Mech. Electron. Opt. Magn. Prop.* **1999**, *79*, 593.

(15) Nakamura, E.; Hirakuri, K. K.; Ohyama, M.; Friedbacher, G.; Mutsukura, N. *J. Appl. Phys.* **2002**, *92*, 3393.

(16) Reinoso, M.; Álvarez, F.; Huck, H. *Appl. Surf. Sci.* **2007**, *254*, 181.

(17) Weiser, P. S.; Prawer, S.; Hoffman, A.; Manory, R. R.; Paterson, P. J. K.; Stuart, S. A. *J. Appl. Phys.* **1992**, *72*, 4643.

(18) Ralchenko, V. G.; Smolin, A. A.; Pereverzev, V. G.; Obraztsova, E. D.; Korotoushenko, K. G.; Konov, V. I.; Lakhotkin, Y. V.; Loubnin, E. N. *Diamond Relat. Mater.* **1995**, *4*, 754.

(19) Silva, F. J. G.; Baptista, A. P. M.; Pereira, E.; Teixeira, V.; Fan, Q. H.; Fernandes, A. J. S.; Costa, F. M. *Diamond Relat. Mater.* **2002**, *11*, 1617.

(20) Bareiss, C.; Perle, M.; Rosiwal, S. M.; Singer, R. F. *Diamond Relat. Mater.* **2006**, *15*, 754.

(21) Polini, R.; Mattei, G.; Valle, R.; Casadei, F. *Thin Solid Films* **2006**, *515*, 1011.

(22) Jao, J. Y.; Han, S.; Chang, L. S.; Chen, Y. C.; Chang, C. L.; Shih, H. C. *Diamond Relat. Mater.* **2009**, *18*, 368.

(23) Galvan, D.; Pei, Y. T.; De Hosson, J. T. M. *Acta Mater.* **2005**, *53*, 3925.

(24) Müller, U.; Falub, C. V.; Thorwarth, G.; Voisard, C.; Hauert, R. *Acta Mater.* **2011**, *59*, 1150.

(25) Silva, F. J. G.; Fernandes, A. J. S.; Costa, F. M.; Baptista, A. P. M.; Pereira, E. *Diamond Relat. Mater.* **2004**, *13*, 828.

(26) Zhang, H. X.; Jiang, Y. B.; Yang, S. Z.; Lin, Z.; Feng, K. A. *Thin Solid Films* **1999**, *349*, 162.

(27) Li, Y. S.; Tang, Y.; Yang, Q.; Xiao, C.; Hirose, A. *Int. J. Refract. Met. Hard Mater.* **2009**, *27*, 417.

(28) Chen, X.; Narayan, J. *J. Appl. Phys.* **1993**, *74*, 4168.

(29) Narayan, J.; Nelson, M.; Oktyabrsky, S.; Jagannadham, K. *Mater. Sci. Eng., B* **1996**, *38*, 46.

(30) Li, Y. S.; Hirose, A. *Surf. Coat. Technol.* **2007**, *202*, 280.

(31) Li, Y. S.; Hirose, A. *Chem. Phys. Lett.* **2006**, *433*, 150.

(32) Li, Y. S.; Yang, Q.; Xiao, C.; Hirose, A. *Thin Solid Films* **2008**, *516*, 3089.

(33) Liu, H. M.; Dandy, D. S. *Diamond Chemical Vapor Deposition: Nucleation and Early Stage Growth Stages*; Noyes Publications: Park Ridge, NJ, 1995; pp 46−78.

(34) Chun, C. M.; Mumford, J. D.; Ramanarayanan, T. A. *J. Electrochem. Soc.* **2002**, *149*, 348.

(35) Egerton, R. F. *Electron Energy-Loss Spectroscopy in the Electron Microscope*, 2nd ed; Plenum Press: New York, 1996.

(36) Ager, J. W.; Drory, M. D. *Phys. Rev. B* **1993**, *48*, 2601.

(37) Yang, Z. Q.; He, L. L.; Zhao, S. J.; Ye, H. Q. *J. Phys.:bCondens. Matter* **2002**, *14*, 1887.

(38) Campbell, T.; Kalia, R. K.; Nakano, A.; Vashishta, P.; Ogata, S.; Rodgers, S. *Phys. Rev. Lett.* **1999**, *82*, 4866.

(39) Campbell, T. J.; Aral, G.; Ogata, S.; Kalia, R. K.; Nakano, A.; Vashishta, P. *Phys. Rev. B* **2005**, *71*, 205413.

(40) Kobashi, K. *Diamond films: Chemical Vapor Deposition for Oriented and Heteroepitaxial Growth*; Elsevier: Amsterdam, 2005; pp 89−116.

(41) Stott, F. H.; Wood, G. C.; Stringer, J. *Oxid. Met.* **1995**, *44*, 113.

(42) Airiskallio, E.; Nurmi, E.; Heinonen, M. H.; Vayrynen, I. J.; Kokko, K.; Ropo, M.; Punkkinen, M. P. J.; Pitkanen, H.; Alatalo, M.; Kollar, J.; Johansson, B.; Vitos, L. *Corros. Sci.* **2010**, *52*, 3394.

(43) Airiskallio, E.; Nurmi, E.; Heinonen, M. H.; Vayrynen, I. J.; Kokko, K.; Ropo, M.; Punkkinen, M. P. J.; Pitkanen, H.; Alatalo, M.; Kollar, J.; Johansson, B.; Vitos, L. *Phys. Rev. B* **2010**, *81*, 033105.

(44) Zhang, Z. G.; Mao, Y. L.; Xie, Y.; Hou, C. M.; Feng, Z. J. *High Temp. Mater. Process* **2010**, *29*, 27.

(45) Heinonen, M. H.; Kokko, K.; Punkkinen, M. P. J.; Nurmi, E.; Kollar, J.; Vitos, L. *Oxid. Met.* **2011**, *76*, 331.

(46) Chen, C. C.; Hong, F. C. N. *Appl. Surf. Sci.* **2005**, *243*, 296.